coatings

MDPI

Article

Improvement of the Tribocorrosion Properties of Cemented Carbide (WC-Tic-Co) Samples with PVD Coating

José Antonio García [1,*], Adrián Claver [1], Mikel Marques [2], Eluxka Almandoz [2], Jonathan Fernández de Ara [2], José F. Palacio [1,2] and Ibon Azkona [3]

[1] Institute for Advanced Materials and Mathematics (INAMAT2), Universidad Pública de Navarra (UPNA), 31006 Pamplona, Spain
[2] Centre of Advanced Surface Engineering (AIN), 31191 Cordovilla, Spain
[3] Metal Estalki, 48170 Zamudio, Spain
* Correspondence: joseantonio.garcia@unavarra.es; Tel.: +34-660-507-256

Abstract: This study aims to investigate the improvement of the tribocorrosion properties of WC-TiC-Co substrates by coating them with hard coatings such as AlCrSiN using cathodic arc deposition. WC-TiC-Co is commonly used in the fabrication of machining and cutting tools; however, there are some materials such as titanium or stainless steel that are difficult to work with; furthermore, in aggressive environments or under high temperatures the performance of the machining tools can be affected, and a failure may occur. This coating is intended to ensure the correct performance of the tools in any conditions. The coatings were characterized by glow discharge optical emission spectroscopy (GDOES), scanning electron microscopy (SEM) and X-ray diffraction (XRD). Tribocorrosion, tribology and corrosion tests were performed to evaluate the tribocorrosion properties of the samples. Furthermore, mechanical and adhesive properties of the coating were studied using scratch and nanoindentation tests. The results showed improved tribocorrosion properties in the samples combined with good adhesive and mechanical properties. These results show the possibility of using these coated materials in the most demanding cutting and machining applications.

Keywords: PVD; tribocorrosion; wear; AlCrSiN; cemented carbide; tribology

Citation: García, J.A.; Claver, A.; Marques, M.; Almandoz, E.; Fernández de Ara, J.; Palacio, J.F.; Azkona, I. Improvement of the Tribocorrosion Properties of Cemented Carbide (WC-Tic-Co) Samples with PVD Coating. *Coatings* **2022**, *12*, 1884. https://doi.org/10.3390/coatings12121884

Academic Editor: Robert J. K. Wood

Received: 6 November 2022
Accepted: 28 November 2022
Published: 4 December 2022

1. Introduction

The current global market for coatings on cutting tools is estimated to be approximately 18 billion dollars. The distribution of the cutting material shows that more than 50% is covered by cemented carbide, and 20% is covered by high-speed steel [1]. In this scenario, CrAlSiN coatings play an important role as they are being widely used for the machining of different materials, i.e., one of its main applications is to coat tungsten carbide tools for the machining of titanium alloys, which are types of material that are difficult to handle, especially at higher cutting speeds. The CrAlSiN coatings show high wear resistances in dry machining of Ti–6Al–4V alloys and excellent cutting performance [2]. Furthermore, given the high oxidation temperature and the excellent chemical stability at elevated temperatures that they present, these coatings are also being applied and tested in high temperature applications [3–6]. More recently, applications for the marine environment were also studied, which is why attention is paid to its resistance to corrosion in environments saturated with NaCl [7].

Indeed, the great interest that these treatments have aroused has also led to the investigation of different architectures over the last two decades (nanocomposites, gradient layers, multilayers, etc.), obtaining very interesting results, both in terms of very high hardness and resistance to wear, as well as resistance to corrosion [8–12].

Moreover, the versatility of these coatings has sparked interest in their possible application in other sectors such as oil and gas, where working conditions are truly extreme, or archaeology, mining industries, oil drilling, etc., where WC-based tools are widely

used and face numerous kinds of corrosive environments: petrochemicals, mine water, lubricants, coolants, cutting fluids and chemically aggressive aqueous media with different pH are extremely corrosive. Thus, it is necessary to complete the behavior studies with tribocorrosion tests where the phenomena of wear and corrosion and their interaction are revealed. In this work we intend to advance in this line by studying the tribocorrosion phenomena of WC substrates coated with CrAlSiN [13].

As was reported in other studies, WC-TiC based materials have shown good wear resistance [14–16] and they are a high-performance and hard substrate for cutting and machining tools. However, they present limited performance on extreme applications. Additionally, it is difficult to measure the hardness of the material due to the distribution of its different phases. Increasing its hardness could be a good strategy to increase the useful life of tools for different processes. Moreover, PVD coatings such as AlCrSiN can improve corrosion resistance of the substrate. AlCrSiN coatings are not as hard as CBN ones, but the hardness of the coating is not the only parameter to take into account. Resistance to oxidation, coefficient of friction and, especially, adhesion are other parameters that must be considered. AlCrSiN coatings have a particularly interesting combination of properties for cutting and machining tool applications. In the specific case of cBN, adhesion presents problems due to the high residual stresses, making it difficult to achieve thicknesses similar to those of AlCrSiN.

This study aims to investigate the tribocorrosion properties of WC-TiC-Co substrates coated with AlCrSiN using a rotatory cathodic arc PLATIT pi80. Tribocorrosion, tribology and corrosion tests were performed to evaluate the resistance to wear, to corrosion and both combined. Furthermore, scratch and nanoindentation tests were carried out to test the surface mechanical properties. Finally, the coatings were characterized by glow dis-charge optical emission spectroscopy (GDOES), scanning electron microscopy (SEM) and X-ray diffraction (XRD) to obtain a fully view of its characteristics.

2. Materials and Methods

2.1. Reference Substrate

Samples of cemented carbide (WC-TiC-Co) quality P-20 (FMD carbide, Basauri, Spain) with flat geometries, 40 mm diameters and 4 mm thickness were used as reference substrates. WC-TiC-Co samples of this quality contain cobalt (Co) as the main binder, and they are composed of other elements such as tantalum niobium carbide (TaNbC) or titanium carbide (TiC). These materials are commonly used in machining of steel with great resistance to high temperatures.

All the samples were subjected to a cleaning and polishing process before the plasma treatment with the objective of achieving a final roughness with an Ra value less than 0.2 µm. Subsequently, the samples were ultrasonically cleaned using alkaline detergents (1% TickopurrR33), rinsed with deionized water, thoroughly cleaned with isopropanol and, finally, air-dried. After the ultrasonic cleaning process, an ion bombardment with Ar within the PVD system at 800V was performed.

2.2. Film Deposition Technique

AlCrSiN coatings were deposited using the technology cathodic arc evaporation. An industrial equipment Platit p80 (Figure 1) (PLATIT AG, Selzach, Switzerland) was used to carry out the process in a vacuum chamber with the following parameters:

- Nitrogen atmosphere at 0.8–2 Pa
- Negative bias voltage of −65 V.
- Cr and Al + Si cathodes as material source.

The deposition process of the AlCrSiN coating with adhesion Cr layer can be found elsewhere [17].

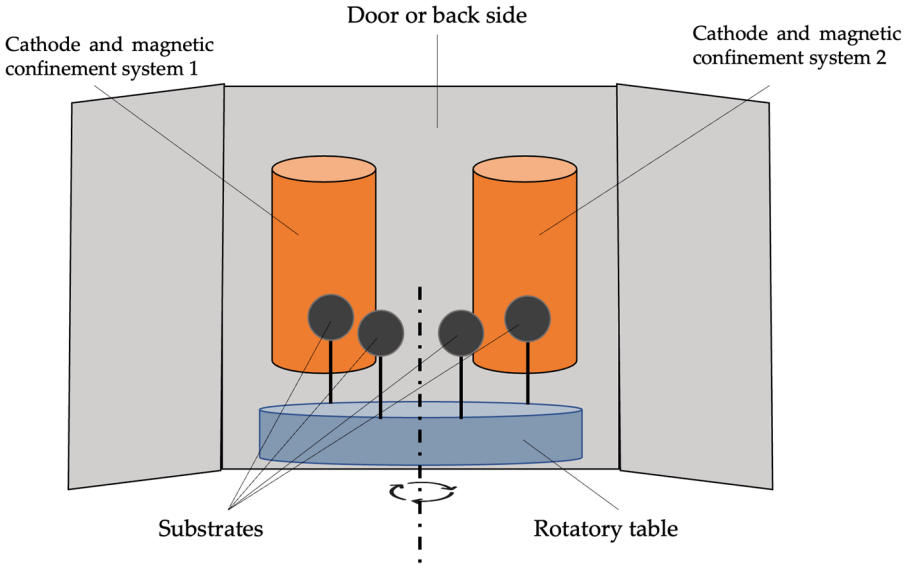

Figure 1. Schematic image of the film deposition process. Inspired by Ref. [18].

2.3. Thickness, Structural Properties and Profile Composition

Glow discharge optical emission spectrometry (GD-OES) was performed with a JOBIN YVON 100000RF GD-OES equipment (HORIBA Instruments, Kyoto, Japan). With this technique, it is possible to analyze the chemical composition profiles and the thickness of the coatings.

Calotest measurements were carried out using a CSM Calotest equipment (CSM Instruments, Needham, MA, USA). This equipment is employed with a 30 mm diameter stainless-steel ball, and the abrasive medium is a superfine (0.25 µm) diamond water suspension. The results obtained by this method are useful to confirm the measured thickness value of the coating.

Finally, a FEI Verios 460 Field Emission XHR-SEM microscope (FEI, Hillsboro, OR, USA) was used to characterize the layers and obtain information about them by obtaining cross-section images.

2.4. Surface and Mechanical Characterization

Adhesion between the substrate and the coating was evaluated by scratch test measurements that were carried out with a CSM REVETEST Scratch tester (Anton Parr, Graz, Austria) and a 200 µm tip radius diamond Rockwell indenter (EURO 150518C&N). For these tests, the following parameters were established: load rate of 100 N/min, a final load of 100 N, a speed of 10 mm/min and a total test length of 10 mm. Using these tests, it is possible to register three different critical loads (Lc) that are related with the adhesion of the coating to the substrate. In order to do this, it is necessary to record different signals such as acoustic emission, friction coefficient or penetration of the indenter within the substrate. Additionally, optical microscopy was used to observe the points where the events occurred. The above-mentioned critical loads are defined in the following lines:

- First critical load (Lc1): it describes the first cohesive failure.
- Second critical load (Lc2): it is associated with the first adhesive failure appearance.
- Third critical load (Lc3): it is registered when total delamination of the coating or a critical defect is observed in a clear way in the reference substrate.

The operation of these tests consists of applying a progressive load on the surface of the specimens through the indenter, and different failure modes will appear at different load values. The first registered failure modes will be those of a cohesive type, such as plastic deformation, or conformal, tensile or lateral type fissurations. This failure mode is associated with the first critical load (Lc1). The second critical load (Lc2) will be registered

when delaminations, superficial lifts, frontal deformation fissurations, or lateral chipping are observed, which are indicative of adhesive-type failure mechanisms.

Finally, the third critical load will be recorded (Lc3), which occurs when it is observed that more than half of the coating is removed from the substrate because the applied load is high enough.

Roughness of the samples (Sa) was measured using a Confocal S Mart Microscope (Sensofar, Barcelona, Spain) with a 20× magnification objective and following the ISO 25178 standard. A surface area of 850.08 μm × 709.32 μm was evaluated in each measurement (three per sample), and the filters that were necessary to apply to obtain the values of the surface roughness are shown:

- Standard cut-off of the high-pass filter (λ_s): 2.50 μm
- Standard cut-off of the high-pass filter (λ_c): 0.08 mm

The hardness and Young's modulus values of the samples were measured by nanohardness measurements. These tests were performed by a MTS NANOINDENTER XP (MTS, Eden Prairie, MN, USA) fitted with a Berkovich tip, with a load function of 0–10,000 μN in 5 s, and a maximum load of 10 mN, and following the Oliver and Pharr method [19] and Bec et al.'s thin film model [20] to correct the influence of the substrate in hardness and Young's modulus. This method uses the approximation of the flat punch model introduced by Sneddon in 1965 [21] and the wear load displacement curves to extract the information of the elastic–plastic characteristics of the materials [19].

2.5. Corrosion and Tribocorrosion Tests

The corrosion resistance of the samples was determined using Electrochemical Tests with an Autolab Potentiostat/Galvanostat PGSTAT302N (Metrohm, Herisau, Switzerland) and the typical three-electrode cell system. For the test materials, with an exposed area of 2 cm^2 served as a working electrode, a silver/silver chloride (Ag/AgCl 3 M) electrode was used as a reference electrode and platinum as the counter one. The samples were immersed in NaCl (1 M) at room temperature to perform the potentiodynamic polarization tests (PDP). Before the tests, the system was stabilized in the solution for 6 min to ensure a stable open circuit potential (OCP); afterwards, the polarization curves were obtained at a range of −250, +750 mV and a scanning rate of 1 mV/s. The Tafel extrapolation method was used to determine the values of Ecorr and icorr from the PDP plots. Electrochemical tests were performed in duplicate to ensure reproducibility.

Tribomechanical tests were carried out using a Microtest MT series equipment (Microtest S.A., Madrid, Spain) in pin-on-disk configuration. In these tests the pins were alumina balls of 6 mm radius, 1650 HV hardness and surface maximum roughness (Ramax) of 0.050 μm. On the other hand, the disks were the tested specimens, that is, coated and uncoated cemented carbide samples. Three tests were performed in each sample at different track radii (8, 12 and 16 mm) but in the same testing conditions: 40 N load, 200 rpm and 20,000 cycles. Wear tracks that were generated during the tests were evaluated by confocal microscopy using a confocal smart microscope (Sensofar, Barcelona, Spain). In this way, volume loss and wear coefficient were determined straight from the confocal measurements and by applying the formula shown in (1). The pin-on-disk system that measures the coefficient of friction collects the force of friction through a load sensor attached to the arm that supports the ball that rotates on the sample to be measured (the typical configuration of these trials). In these tests, it is usual to have variations in the coefficient of friction throughout the test (fundamentally at the beginning) as the contacts between the ball and the disk are accommodated. The variations that are shown in these tests may be due to several complex phenomena such as the appearance of third particles, formation of oxide layers, etc.

$$\frac{\text{V loss confocal } (\text{m}^3)}{\text{wear track length } (\text{m})} \times 2 \times \Pi \times \text{r } (\text{m}) = \text{V loss } (\text{m}^3) \quad (1)$$

The tribocorrosion behavior of uncoated and coated samples was evaluated in NaCl (1 M) by tribocorrosion tests that were performed in modified pin-on-disc equipment (Microtest, Madrid, Spain) integrated with an electrochemical workstation (Metrohm, Herisau, Switzerland). A scheme of the set-up used in this study is shown in Figure 2. A three-electrode system was established using uncoated and coated samples as the working electrode, a Pt gauze as the counter electrode and an Ag/AgCl electrode as the reference electrode. Friction test parameters were as follows: 40 N load, 100 rpm, 8 mm radius and 6mm radius ruby ball as counterpart. The interaction between wear and corrosion was evaluated by potentiodynamic polarization tests (PDP) with sliding that were compared with the PDP tests that were performed without sliding. The specimens were immersed in the solution to stabilize the open circuit potential (OCP), and OCP was measured before and after sliding. PDP tests were performed at a scan rate of 1 mV/s and a range of −250, +750 mV. Tafel extrapolation method was used to determine the values of Ecorr and icorr from the PDP plots.

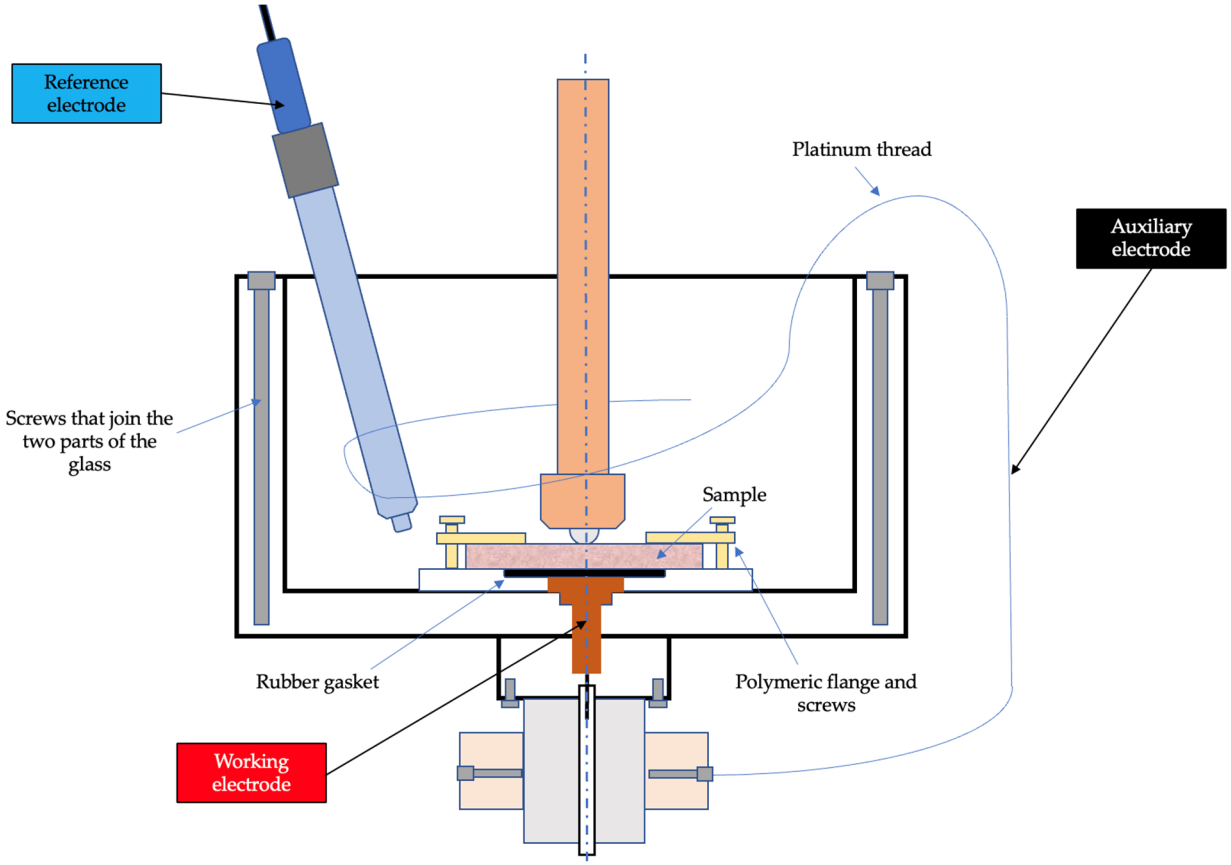

Figure 2. Set-up of the tribocorrosion tests performed combining pin-on-disk and potentiodynamic polarization tests.

3. Results

3.1. Thickness, Structural Properties and Profile Composition

The chemical composition profile and the resultant thickness of the coating were determined by GD-OES; the results are shown in Figure 3. The PVD coated sample showed an outermost layer of about 3.5 µm composed of approximately 55% N, 30% Cr, 20% Al and 2% Si. Following this layer, it is possible to observe a small increase in the percentage of Cr, which is related to the transition layer and the CrN anchoring layer that is deposited to improve the affinity of the coating with the substrate and, thus, the adhesion. Regarding the substrate, its composition is mainly composed of carbon, tungsten, cobalt, and titanium.

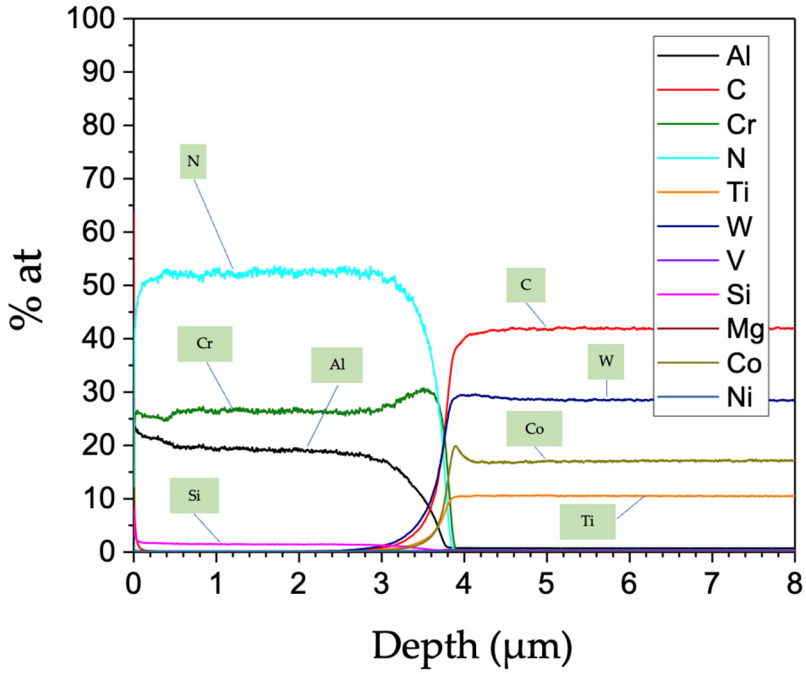

Figure 3. Glow discharge optical spectrometry (GD-OES) concentration profiles in the AlCrSiN coated WC-TiC-Co sample.

The results of the calotest measurements that were performed to corroborate the GD-OES results are shown in Table 1. The 3 different layers that were mentioned in the GD-OES results are also shown in this test, anchoring layer, transition layer and an outer layer. The anchoring layer of CrN presented a thickness of approximately 0.25 μm, followed by a thicker transition layer and an AlCrSiN outer layer of more than 4 μm. In this case, the resultant thickness of the whole coating was slightly thicker than in the GD-OES results, 4.5 μm, but it must be considered that the thickness observed in the GD-OES measurements is an approximation.

Table 1. Thickness of each layer measured by calotest.

Anchoring layer	0.25 μm
Transition layer + outer layer	4.25 μm
Total thickness	4.5 μm

The surface of the uncoated WC-Co and AlCrSiN samples obtained by SEM are shown in Figure 4. In the case of the uncoated sample (Figure 4a), a typical microstructure of grains in the two phases of WC and TiC alloys can be seen, similar to those reported in studies such as [22]. On the other hand, the AlCrSiN coating presented a surface morphology with a homogeneous structure with a small number of droplets due to the polishing final treatment after the PVD process. Droplet generation is common in cathodic arc coating processes. In this case, the coatings have a low number of microdroplets due to two factors: on the one hand, the rotating cathode system of the pi80 equipment minimizes these defects due to its unique design, and on the other hand, a final polishing is performed after coating deposition.

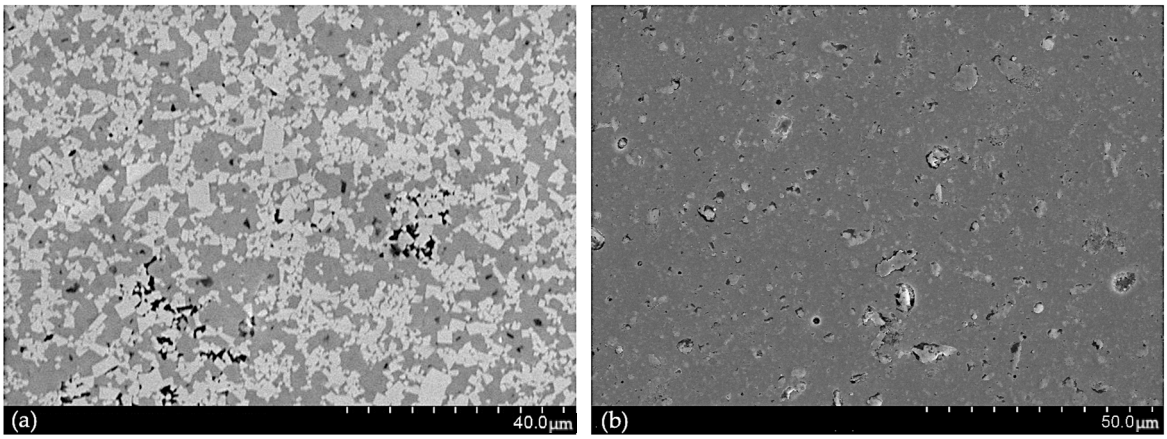

Figure 4. SEM images of the surface of the polished WC-TiC-Co uncoated sample (**a**) and AlCrSiN coated sample (**b**).

Figure 5 shows the cross-section SEM pictures of the coating, where the different layers observed in the GD-OES and calotest are schematically indicated. The anchoring layer of approximately 0.25 µm is followed by the transition and the outer layer, with a total coating thickness of approximately 4.5 µm. As it was reported in [23], the AlCrSiN coating presented a refined grain and a face-centered cubic (FCC)-type structure.

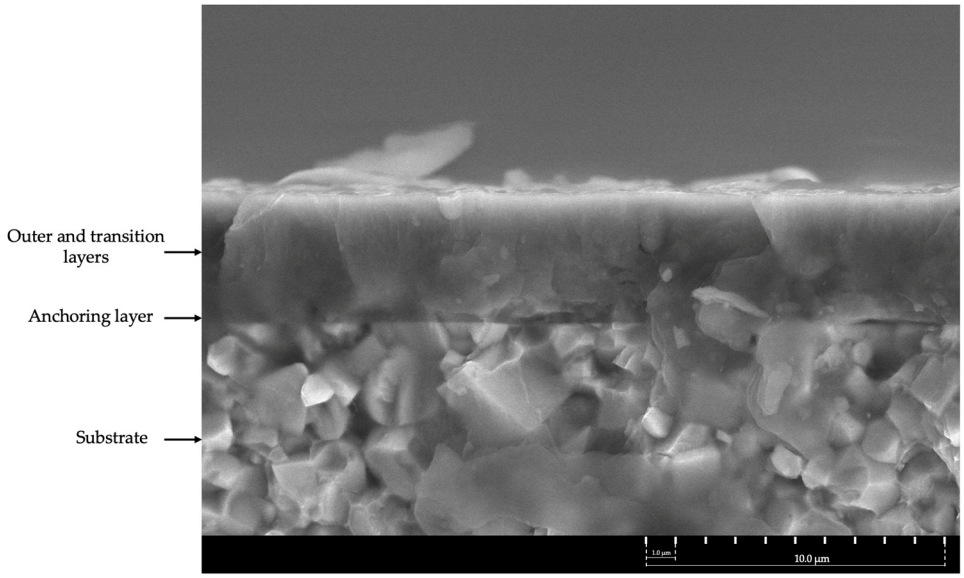

Figure 5. Cross-section SEM image with the AlCrSiN coating's structure in the WC-TiC-Co substrate.

3.2. Surface and Mechanical Characterization

In PVD processes, roughness is a critical parameter for achieving good adhesion between substrate and coating [24]; moreover, corrosion and wear resistance of the samples are influenced by their surface finish [25,26]. Sa (arithmetical mean height) of the specimens was measured in three different zones of the surface to determine their surface finish and observe possible differences between the surfaces before and after the deposition process. The uncoated samples presented a Sa value of 19 $\pm$ 1 nm, while the AlCrSiN coated sample presented a value of 50 $\pm$ 2 nm. In both cases the measured roughness value was low enough to consider smooth with a good surface finish, but the increase observed in the case of the coated sample can be a consequence of the microdroplets that were observed in the SEM characterization.

Nanoindentation tests provide information about hardness, Young's modulus, and resistance to plastic deformation in the coated and uncoated samples; the results are summarized in Table 2. For the uncoated samples, it must be noted that there are three different phases: WC, TiC and the cementant Co, so their microstructure determines that they presented nanoindentation tests results that are clearly grouped into three differentiated populations. As can be seen, the hardness of the coated samples is greater than that presented by the uncoated sample while the Young's modulus of uncoated samples is similar or slightly greater (TiC) than that of the coated ones. The relation between hardness and Young's modulus is represented by H^3/E^2 and H/E, which are related to resistance to plastic deformation in loaded contact and elasticity, respectively [27,28]. Increasing the ratio H^3/E^2 could lead to an improvement in the elastic recovery of the coating, since it is related to the elastic limit of the material and toughness [28–30]. Furthermore, different research works have shown that resistance to various forms of wear is correlated with this ratio [31–33]. Toughness is an important parameter in tribological applications, and as many studies have reported, H/E and H^3/E^2 can be more important than just hardness to determine the wear resistance properties of a material [27,28,34].

Table 2. Hardness, Young's modulus and relation between both values measured in the nanoindentation tests for coated and uncoated samples.

Sample	Hardness (Gpa)	Young's Modulus (Gpa)	H/E	H^3/E^2
Coated sample	34.1 ± 6.6	301 ± 35	0.113	0.438
Uncoated P1 (TiC)	26.4 ± 2.5	310 ± 8.5	0.085	0.191
Uncoated P2 (WC)	19.6 ± 1.8	302 ± 14.8	0.064	0.082
Uncoated P3 (WC′)	13.8 ± 1.0	270 ± 2.2	0.051	0.036

In this study, coated samples presented greater values in both cases, H^3/E^2 and H/E, whereas it was concluded in many studies that an increase in these values supposes a greater resistance to plastic deformation and wear. Hardness values measured for the uncoated WC-TiC-Co samples are similar to those reported in other studies [35–37]. The results of hardness and H^3/E^2 reported for the AlCrSiN, instead, are similar and even higher than those presented in other research, such as AlCrN/AlCrSiN coatings deposited on high-speed steels [38], carbide cutting tools coated with TiAlN/TiSiN and monolayer AlCrSiN ceramic films [39] or AlCrSiN and AlCrSiON deposited on cemented carbide substrates [40]. The higher values of H^3/E^2 are an indicator of a higher resistance to plastic deformation and improved wear resistance of the coating if it is compared with the uncoated WC-TiC-Co. These properties are very important in high demanding applications where tools are subjected to high loads, wear, and corrosive environments, such as mining industries, rock industries or petrochemicals [13].

Load–unloading curves that show the plastic and elastic work of the materials are shown in Figure 6. The linear behavior in the middle to end of a load curve for an uncoated material can be attributed to a compaction of porous material, with the contact area being constant with load [41]. In the case of a coated material, the presence of cracks at the interface causes the coating to detach and behave elastically similar to a membrane, which is also reflected linearly in the final part of the load curve [42].

Scratch tests were performed on the coated samples in order to obtain information about the adhesion of the coating to the substrate and its mechanical response. Figure 7 shows an example of the results obtained for the AlCrSiN coated WC-TiC-Co sample after a scratch test. For determining the critical loads values where failures occurred (cohesive, adhesive, or total failure) the scratches were observed to evaluate the different failure modes. Furthermore, it was necessary to observe spontaneous changes in the COF evolution plot and sharp rises in the acoustic emission signal.

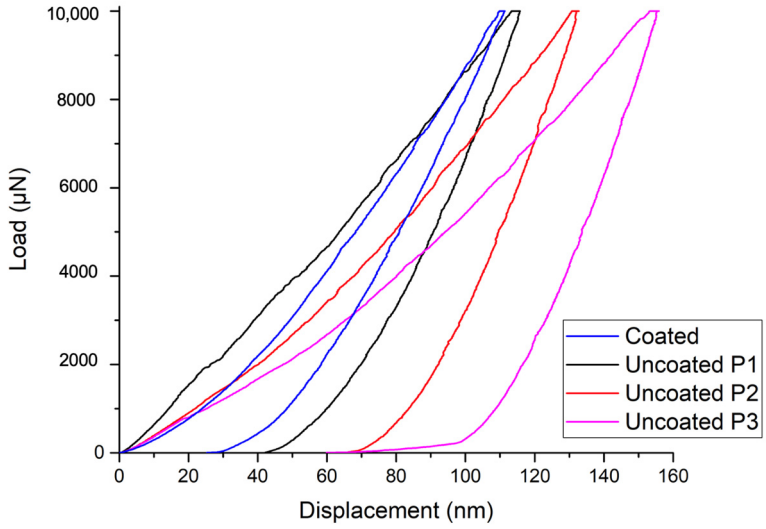

Figure 6. Loading–unloading curves of the coated and uncoated samples after nanoindentation tests.

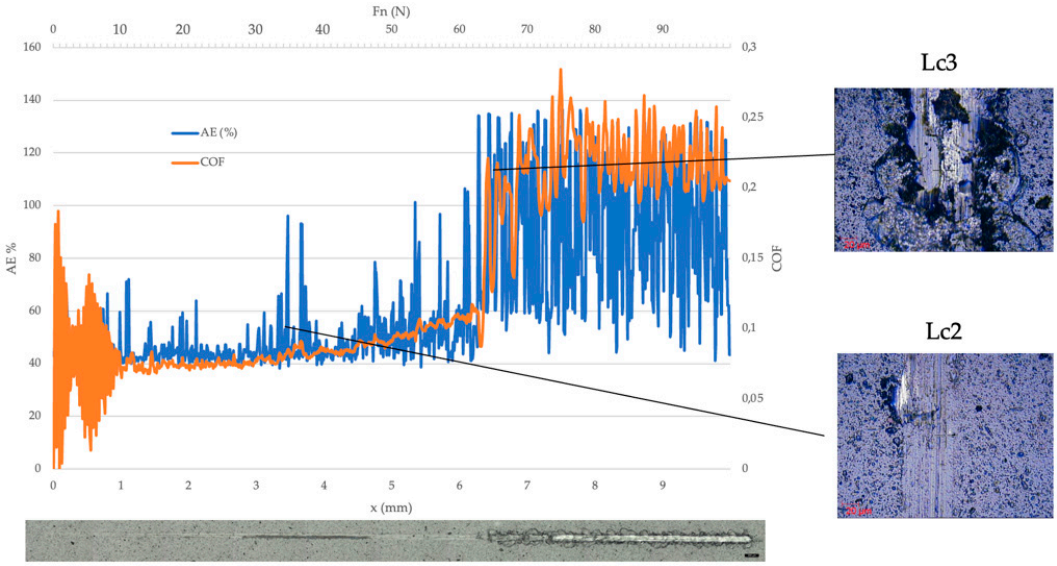

Figure 7. Scratch test results for the coated WC-TiC-Co samples. Evolution of the coefficient of friction (orange plot) and acoustic emission (blue plot) vs. the indenter displacement and the normal force, scratch obtained after the test and images of the zones of the track where critical loads Lc2 and Lc3 were recorded.

As was mentioned before, there are three critical loads that represent the different failure mechanisms, cohesive failure (Lc1), adhesive failure (Lc2) and appearance of the substrate (Lc3). Analyzing the values observed for these loads, it is possible to analyze the adhesion of the coating to the substrate, while higher values of critical loads suppose greater adhesion to the substrate. The results of critical loads obtained for the coated samples are summarized in Table 3. First of all, it can be seen that no cohesive failure was observed in the coated samples scratch tests. On the other hand, the first adhesive failure was observed at a load of 33.3 N, while the appearance of the substrate occurred at approx. 63.7 N. To obtain these adhesion values on substrates such as WC-TiC-Co, an ionic cleaning process was carried out followed by a CrN anchoring layer. Surface preparation of the substrate is a critical factor in the final adhesion of the coating, so cleaning and preparing it for achieving a good final finish is a very important factor. The anchoring layer, on the other hand, can reduce the internal stresses generated in the substrate-coating interface

and improve chemical affinity, improving the adhesion of the coating to the substrate and minimizing the appearance of adhesive defects.

Table 3. Critical load values (Lc2 and Lc3) measured in the scratch tests.

Critical Load	Value
Lc2	33.3 ± 1.5 N
Lc3	63.7 ± 4.9 N

Zhang et al. reported similar results; Lc2 values between 40 and 60 N, for CrAlSiN coatings deposited on cemented carbide substrates with a similar percentage of Co in the chemical composition, using multiarc ion plating [43]. Lower values of both Lc2 and Lc3 were reported for multilayer PACVD coatings deposited on nanostructured WC-Co cemented carbides [44]. Sezer çam et al., instead, presented values of critical loads of approximately 90–100 N for CrAlSiN and TiAlN/TiSiN coatings deposited on tungsten carbide (WC–12Co) by cathodic arc physical vapor deposition [39]. Differences in the chemical composition of the substrate, and therefore, in its mechanical properties, and the droplets that were observed on the surface of the coated samples could explain the lower critical load values observed in this study if they are compared with [39].

3.3. Corrosion and Tribocorrosion Tests

Friction and wear properties of the AlCrSiN coatings and WC-TiC-Co substrates were studied by pin-on-disc tests prior to tribocorrosion tests to obtain information about the wear resistance of the samples in dry conditions. Graphs of the coefficient of friction (COF) obtained from the wear test are shown in Figure 8. As could be expected, since these coatings are not low friction coatings, COF values were similar for uncoated and coated samples, and they presented values of around 0.6 in both cases for dry conditions. Nonetheless, wear resistance is different for each sample and the results measured following the standard ASTM G99 and straight from confocal measurements can be observed in Figure 9. The evaluation of volume loss and wear coefficient were carried out using these two methods to obtain the most precise information that could be obtained and to be able to compare both methods of measurement [45]. The results obtained by both methods showed that wear coefficient (K) was lower for the AlCrSiN coated samples than for the uncoated ones. A lower value of K implies a greater wear resistance, so as it can be seen, the uncoated samples presented values of approximately 5×10^{-5} mm^3/Nm (ASTM G99) and 1.7×10^{-5} mm^3/Nm (confocal), while the coated samples presented values of 4×10^{-5} mm^3/Nm (ASTM G99) and 1.8×10^{-7} mm^3/Nm (confocal). The improved wear resistance presented by coated samples is consistent with the results observed in nanoindentation tests, where resistance to plastic deformation; determined by H^3/E^2, is also greater in these samples. Other studies have reported improved wear resistance by depositing PVD coatings on tungsten carbides [2,39]. However, the wear coefficient results obtained in this study are lower than those presented for other PVD coated cemented carbides [2] or advanced cemented tungsten carbides [46], which suggests an improvement in the wear resistance of tungsten carbides.

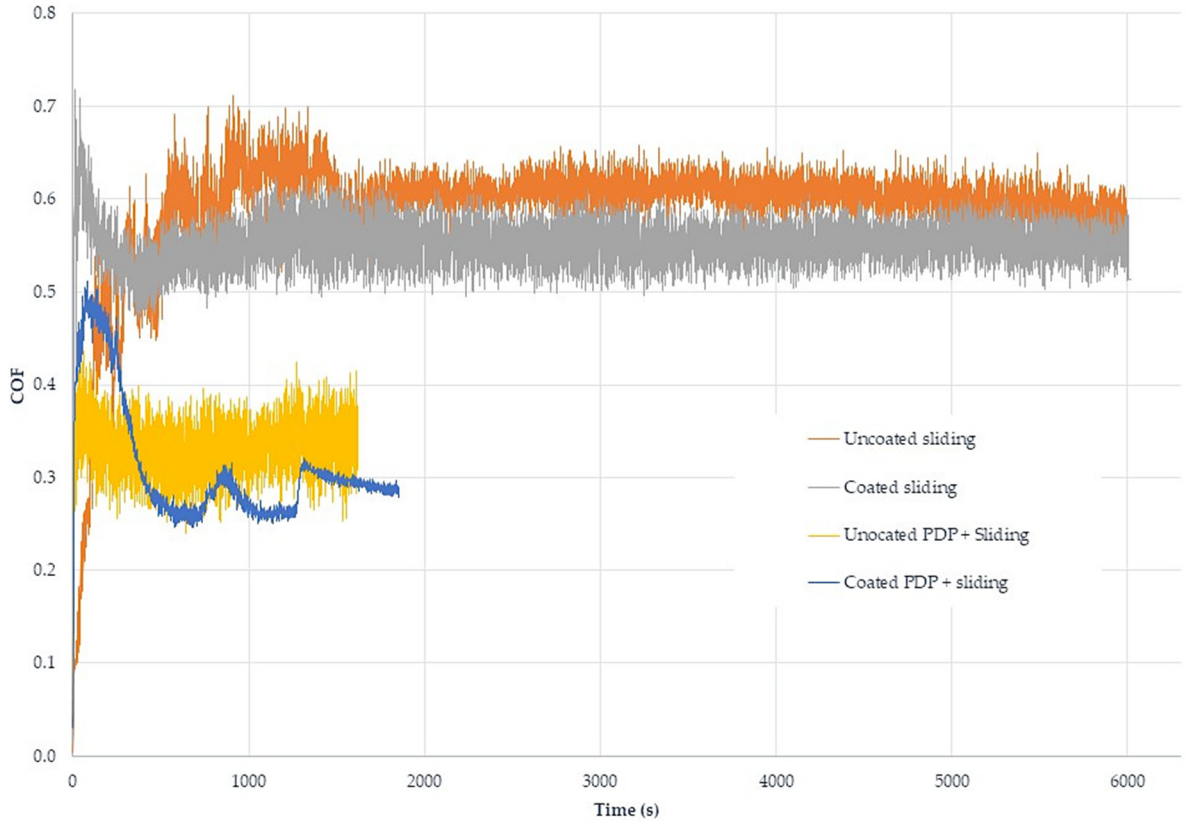

Figure 8. Friction coefficient of coated and uncoated simples in dry conditions and in combinate tests of PDP and sliding.

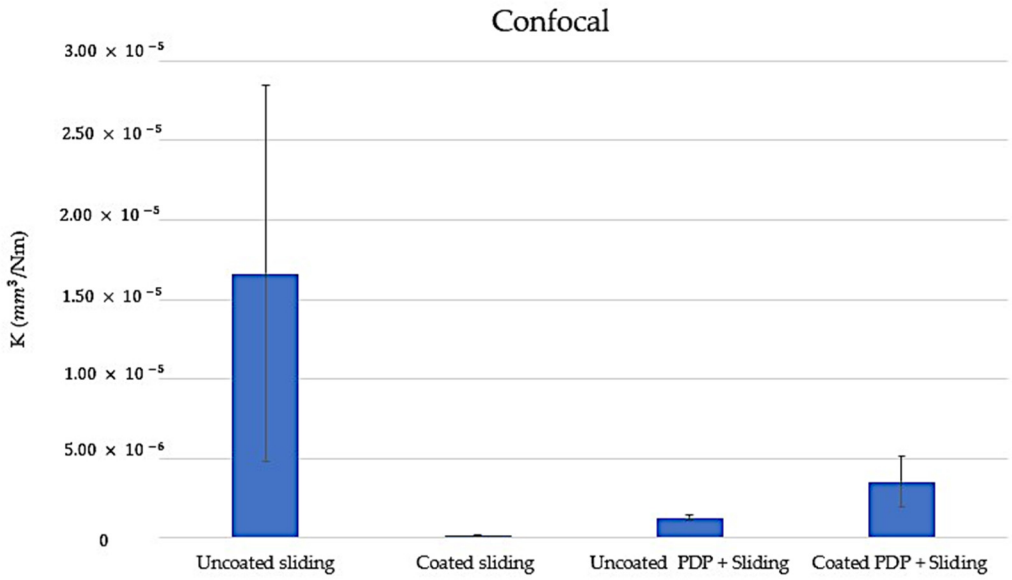

Figure 9. Wear coefficient (K) values measured straight from the volume loss values measured by confocal microscopy for both coated and uncoated samples in dry conditions.

Important differences were observed in wear and corrosion resistance behavior of the samples when wear and corrosion tests were combined. The measured COF value remained similar in both cases, uncoated and coated samples, but it decreased to a value of approximately 0.3–0.35. This reduction in COF was produced because the thin fluid film of NaCl present in the surface of the samples worked as a weak lubricant, and the tribolayer formed during the process served to reduce the contact pressure [47,48]. Coated

samples presented fluctuations while varying the potential in potentiodynamic polarization, whereas COF maintained stability in uncoated samples. In the case of the coated sample, the measured wear coefficient value increased to 3.5×10^{-6} mm^3/Nm due to the combination of wear and corrosion. As was shown in other studies, the corrosion process habitually accelerates the wear process, increasing wear coefficient value and, therefore, worsening the wear resistance of coatings or substrates [49,50]. On the other hand, uncoated samples presented similar values than those of the coated ones and lower than those measured in dry conditions, approximately 1.3×10^{-6} mm^3/Nm. The decrease in the wear coefficient value of uncoated samples could be due to the presence of an oxide layer generated during the combined PDP and sliding tests and the generation of corrosion and wear products that were deposited into the wear track [51]. As mentioned, wear is measured by evaluating the volume loss from the groove in the pin on disk tests using confocal microscopy. The reduction in wear coefficient (k) is due to the increased hardness of the surface and, therefore, to an increase in the resistance to abrasion, since the abrasive wear depends mainly on the ratio of hardness between the surfaces in contact.

Figure 10 shows images of wear tracks obtained by confocal microscopy for coated and uncoated samples in both dry and tribocorrosion conditions. These images are obtained together with the measurements in the volume loss that help us to have a first evaluation of the wear characteristics. With these images, it is possible to show differences between wear mechanisms that are present in each test, so that it is possible to corroborate the wear coefficient results and obtain more information about the performance of the coating. If different types of wear presented in each sample are observed, in dry conditions (Figure 10a,b), uncoated samples presented dipper wear tracks with mostly adhesive wear. Coated samples, instead, presented less wear and typical microscratches that are related with abrasive wear. The images obtained after the tribocorrosion tests (Figure 10c,d) showed that in both cases samples suffered greater wear and their surface is considerably more damaged.

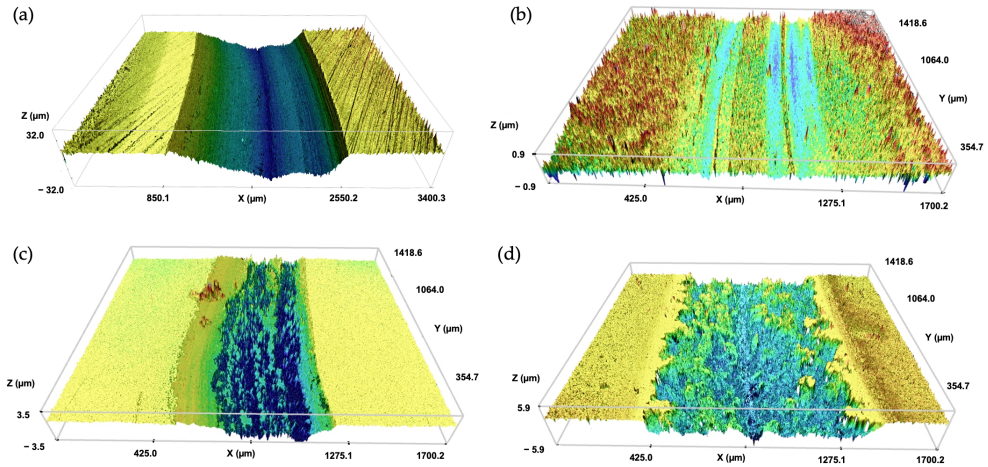

Figure 10. Images of the wear tracks obtained by confocal microscopy for uncoated WC-TiC-Co samples sliding in dry conditions (**a**) and in NaCl solution (**c**), and AlCrSiN coated samples in dry conditions (**b**) and in NaCl solution (**d**).

Figure 11 shows the potentiodynamic polarization curves obtained from the electrochemical tests for the coated and uncoated samples with and without sliding. As can be seen, current fluctuations are considerably more pronounced when wear and corrosion occur simultaneously (green and yellow plots).

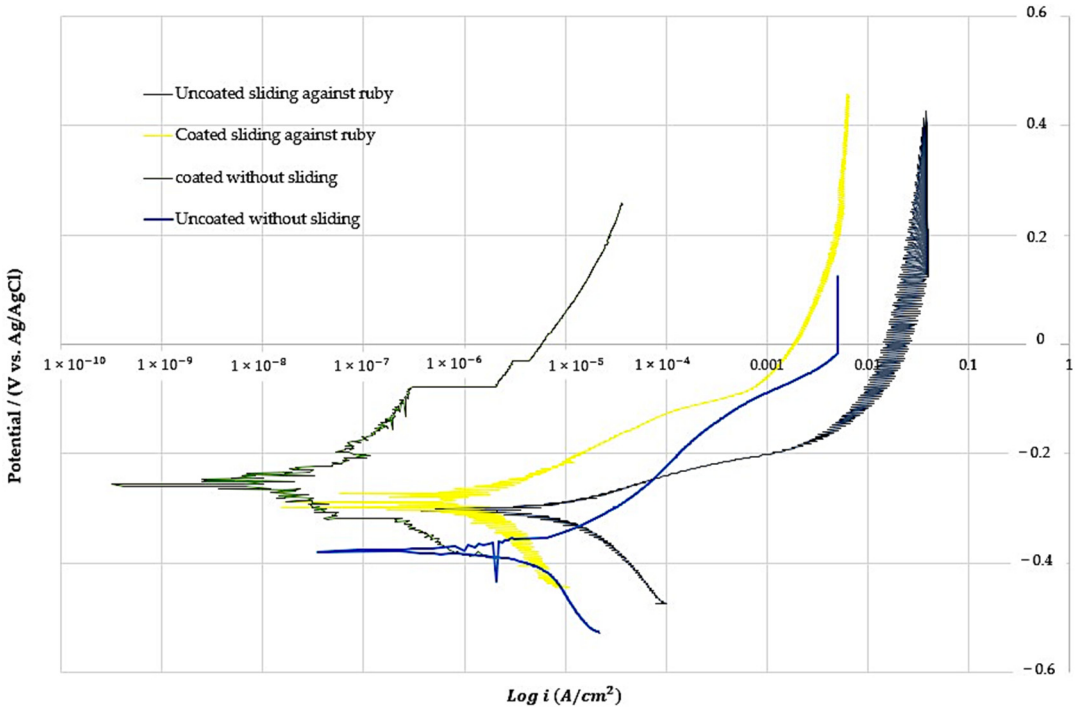

Figure 11. Potentiodynamic polarization plots obtained for uncoated and coated samples with and without sliding against ruby balls.

Corrosion potential (Ecorr) and current density were obtained through Tafel slope extrapolation, and they are presented in Table 4. A decrease in the value of current density is associated with higher corrosion resistance, and more positive corrosion potential is indicative of a reduction in corrosion initiation tendency because of the retardment of anodic kinetics [52]. In this case, it can be seen that current density is reduced in the coated samples both for sliding and no-sliding conditions. The lowest value of current density was observed for the coated sample without sliding, 0.03 μA/cm^2, while when PDP tests were performed in combination with sliding, the value increased to 0.36 μA/cm^2. The highest value, which is related with the worst corrosion resistance, was observed for the uncoated sample sliding against the ruby ball (8.56 μA/cm^2).

Table 4. Potential and current density values obtained from the potentiodynamic polarization tests for uncoated and coated samples with and without sliding against ruby balls.

Sample	Corrosion Potential (V)	Current Density (μA/cm^2)
Uncoated without sliding	−0.38	1.11
Coated without sliding	−0.26	0.03
Uncoated sliding against ruby	−0.31	8.56
Coated sliding against ruby	−0.29	0.36

Corrosion potential shifted to more positive values in the coated samples, and the differences were especially appreciable in the tests that were performed without sliding. The results obtained for Ecorr and current density showed an improvement in the corrosion resistance of AlCrSiN coated samples compared to uncoated ones. Although this result should be studied in greater depth, some causes can be pointed out for this increase in corrosion resistance. One of them would be that the AlTiSiN layers are homogeneous on the surface and do not present segregations or differentiated phases, such as in the case of uncoated WC-TiC-Co substrates. In addition, the barrier effect must be considered. As it is a coating with resistance to corrosion, due to its composition, and having shown a

homogeneous surface practically without defects, those microns of layer deposited on the surface of the substrate increase the useful life of the material, protecting it from degradation by corrosion.

The results obtained for the uncoated samples are similar to those reported by other authors where the corrosion resistance of Co-based cemented carbides was evaluated [22,53]. Other studies have shown the efficacy of PVD coatings in improving corrosion resistance in cemented carbides [13,43], while the tribocorrosion behavior is still a subject that must be studied in depth that does not have many studies related to it.

4. Discussion

Once all the tests and results are presented, it is possible to comment and discuss some aspects concerning them. First of all, it is important to mention that the substrates employed in this study, cemented carbides, present good corrosion and wear resistance properties, so the objective of this study was to improve even more these properties for extreme applications where they are not able to withstand the tribocorrosion requirements.

As can be seen in the SEM images of the uncoated sample, there are three different phases: WC, TiC and the cementant Co. This microstructure determines that the nanoindentation tests at 10 mN of the final load gave results that were grouped into three clearly differentiated populations. The hardest TiC precipitates offer nanohardness results of approximately 26 GPa, while for those of WC, the results were approximately 20 and 14 GPa. Nominally, the TiC precipitates should offer hardness above 30 GPa and those of WC hardness, just over 15 GPa. This variation with respect to the nominal values is a consequence of the interaction of the three phases present in the material and the difficulty of indenting in one phase without affecting the other present phases.

Under these conditions, it is difficult to establish a clear relationship between the H/E and H^3/E^2 parameters that allows us to obtain information on the wear resistance of the base material. In other words, taking the H and E values of the WC as a reference without taking into account the reinforcing effect of the TiC particles to try to establish relationships between the wear of the uncoated sample leads to important errors. In addition, materials reinforced with ultra-hard phases such as TiC provide an extra effect of resistance to abrasive wear that is not considered when trying to draw conclusions from the relationships between H, E and the wear coefficient.

In any case, the wear resistance of the coated samples increases considerably with respect to the uncoated samples, reducing the K by two orders of magnitude. However, the wear in the tribocorrosion tests is very similar in the coated and uncoated samples, probably due to the appearance of oxides with a lubricating effect in the uncoated samples. In addition, it seems that in the coated samples, delamination of the coating may possibly occur due to damage to the hard metal substrate, specifically due to an attack on the hard metal-coating interface that makes it lose its support. This phenomenon is not very common in the cutting applications for which this gradient type coating is designed.

The potentiodynamic polarization tests indicated that the AlCrSiN coating improved the corrosion resistance of the substrate, since the results showed that with the coating, the corrosion potential shifted to more positive values, which is related to the reduction in corrosion initiation tendency, and current density was reduced in both sliding and static PDP tests. This improvement was especially evident in the tests that were performed without sliding.

Despite the good results obtained, it would be necessary to study in deeper some aspects such as the improvement of the adhesion of the coating or avoiding the loss of wear resistance when combining wear and corrosion.

The AlCrSiN coating that was deposited in this study is a very good option for applications where cemented carbides work in extreme dry conditions, where high loads are expected. Furthermore, in applications that combine high loads and wear and a corrosive environment, the coating has shown that it still improves corrosion resistance in the substrate and maintains good wear resistance. Therefore, AlCrSiN coating de-

posited by cathodic arc evaporation could be a promising option for cemented carbide tools working in either dry or wet conditions that require even better wear and corrosion resistance properties.

5. Conclusions

TiAlSiN coatings by cathodic arc made on WC-TiC-Co substrates of more than 4.5 microns offer hardnesses of more than 30 GPa. The adhesions achieved are within the expected range and consistent with those found in similar studies.

Although this substrate is characterized by a high resistance to wear, through the coating, it was possible to reduce wear by two orders of magnitude.

The corrosion resistance in the substrate was improved in both dry and tribocorrosion conditions, as was shown by the potentiodynamic polarization tests. These results were especially appreciable in dry conditions.

The tribocorrosion tests indicate that the wear of the coating is due to the failure of adhesion of the interface. This aspect should be studied in depth in future studies to try to achieve even better results that allow extending the useful life of tools in the most extreme conditions.

The AlCrSiN coating deposited by cathodic arc evaporation could be a promising option for cemented carbide tools, especially in dry conditions, but also in extreme applications that combine wear and corrosion.

Author Contributions: Conceptualization, J.A.G., A.C., E.A., J.F.P. and I.A.; methodology, J.A.G., A.C., M.M. and E.A.; investigation, J.A.G., A.C., E.A., J.F.d.A., J.F.P. and M.M.; resources, J.A.G., A.C., E.A. and I.A.; data curation, J.A.G., A.C. and E.A.; writing—original draft preparation, J.A.G., A.C., E.A., J.F.P. and I.A.; writing—review and editing, J.A.G., A.C., E.A. and I.A.; supervision, J.A.G. and E.A.; project administration, J.A.G. and E.A.; funding acquisition, J.A.G. and E.A. All authors have read and agreed to the published version of the manuscript.

Funding: Funded in part by the Spanish Ministry of Science, Innovation and Universities through grant PGC2018-096855-B-C43 and PGC2018-096855-A-C44.

Institutional Review Board Statement: Not applicable.

Informed Consent Statement: Not applicable.

Data Availability Statement: Not applicable.

Conflicts of Interest: The authors declare no conflict of interest.

References

1. Bobzin, K. High-Performance Coatings for Cutting Tools. *CIRP J. Manuf. Sci. Technol.* **2017**, *18*, 1–9. [CrossRef]
2. Chang, Y.Y.; Lai, H.M. Wear Behavior and Cutting Performance of CrAlSiN and TiAlSiN Hard Coatings on Cemented Carbide Cutting Tools for Ti Alloys. *Surf. Coat. Technol.* **2014**, *259*, 152–158. [CrossRef]
3. Shieh, Y.N.; Chang, Y.Y. Influence of Cobalt Ion Implantation on Optical Properties of Titanium Dioxide Thin Films. *Thin Solid Films* **2010**, *518*, 7464–7467. [CrossRef]
4. Thobor-Keck, A.; Lapostolle, F.; Dehlinger, A.S.; Pilloud, D.; Pierson, J.F.; Coddet, C. Influence of Silicon Addition on the Oxidation Resistance of CrN Coatings. *Surf. Coat. Technol.* **2005**, *200*, 264–268. [CrossRef]
5. Chang, Y.Y.; Chang, C.P. High Temperature Stability of Multicomponent TiAlSiN and CrAlSiN Coatings. *J. Nanosci. Nanotechnol.* **2010**, *10*, 4762–4766. [CrossRef]
6. Chang, Y.Y.; Cheng, C.M.; Liou, Y.Y.; Tillmann, W.; Hoffmann, F.; Sprute, T. High Temperature Wettability of Multicomponent CrAlSiN and TiAlSiN Coatings by Molten Glass. *Surf. Coat. Technol.* **2013**, *231*, 24–28. [CrossRef]
7. Sun, S.Q.; Ye, Y.W.; Wang, Y.X.; Liu, M.Q.; Liu, X.; Li, J.L.; Wang, L.P. Structure and Tribological Performances of CrAlSiN Coatings with Different Si Percentages in Seawater. *Tribol. Int.* **2017**, *115*, 591–599. [CrossRef]
8. Wu, W.; Chen, W.; Yang, S.; Lin, Y.; Zhang, S.; Cho, T.Y.; Lee, G.H.; Kwon, S.C. Design of AlCrSiN Multilayers and Nanocomposite Coating for HSS Cutting Tools. *Appl. Surf. Sci.* **2015**, *351*, 803–810. [CrossRef]
9. Zhang, Y.F.; Yan, W.Q.; Chen, L.; Liao, B.; Hua, Q.S.; Zhang, X. A Hard yet Tough CrAlSiN Nanocomposite Coating for Blades Deposited by Filtered Cathode Vacuum Arc. *Surf. Interfaces* **2021**, *25*, 101156. [CrossRef]
10. Chen, J.K.; Chang, C.L.; Shieh, Y.N.; Tsai, K.J.; Tsai, B.H. Structures and Properties of (TiAlSi)N Films. *Procedia Eng.* **2012**, *36*, 335–340. [CrossRef]

11. Hu, J.; Zhang, J.; Jiang, Z.; Ding, X.; Zhang, Y.; Han, S.; Sun, J.; Lian, J. Plastic Deformation Behavior during Unloading in Compressive Cyclic Test of Nanocrystalline Copper. *Mater. Sci. Eng. A* **2016**, *651*, 999–1009. [CrossRef]
12. Tao, H.; Tsai, M.T.; Chen, H.W.; Huang, J.C.; Duh, J.G. Improving High-Temperature Tribological Characteristics on Nanocomposite CrAlSiN Coating by Mo Doping. *Surf. Coat. Technol.* **2018**, *349*, 752–756. [CrossRef]
13. Bilgin, S.; Güler, O.; Alver, Ü.; Erdemir, F.; Aslan, M.; Çanakçı, A. Effect of TiN, TiAlCN, AlCrN, and AlTiN Ceramic Coatings on Corrosion Behavior of Tungsten Carbide Tool. *J. Aust. Ceram. Soc.* **2021**, *57*, 263–273. [CrossRef]
14. Chen, L.; Zhao, Y.; Meng, F.; Yu, T.; Ma, Z.; Qu, S.; Sun, Z. Effect of TiC Content on the Microstructure and Wear Performance of in Situ Synthesized Ni-Based Composite Coatings by Laser Direct Energy Deposition. *Surf. Coat. Technol.* **2022**, *444*, 128678. [CrossRef]
15. Chen, L.; Yu, T.; Guan, C.; Zhao, Y. Microstructure and Properties of Metal Parts Remanufactured by Laser Cladding TiC and TiB_2 Reinforced Fe-Based Coatings. *Ceram. Int.* **2022**, *48*, 14127–14140. [CrossRef]
16. Zhao, Y.; Yu, T.; Sun, J.; Jiang, S. Microstructure and Properties of Laser Cladded B4C/TiC/Ni-Based Composite Coating. *Int. J. Refract. Metals Hard Mater.* **2020**, *86*, 105112. [CrossRef]
17. Mosquera, A.; Mera, L.; Fox-Rabinovich, G.S.; Martínez, R.; Azkona, I.; Endrino, J.L. Advantages of Nanoimpact Fracture Testing in Studying the Mechanical Behavior of Cral(Si)n Coatings. *Nanosci. Nanotechnol. Lett.* **2010**, *2*, 352–356. [CrossRef]
18. PLATIT. Advanced Coating Systems Nanostructured Coatings for High Per-Formance Tools. *Reprint Werkzeug Tech.* **2003**, *77*, 2–7.
19. Oliver, W.C.; Pharr, G.M. An Improved Technique for Determining Hardness and Elastic Modulus Using Load and Displacement Sensing Indentation Experiments. *J. Mater. Res.* **2011**, *7*, 1564–1583. [CrossRef]
20. Bec, S.; Tonck, A.; Loubet, J.L. A Simple Guide to Determine Elastic Properties of Films on Substrate from Nanoindentation Experiments. *Philos. Mag.* **2006**, *86*, 5347–5358. [CrossRef]
21. Sneddon, I.N. The Relation between Load and Penetration in the Axisymmetric Boussinesq Problem for a Punch of Arbitrary Profile. *Int. J. Eng. Sci.* **1965**, *3*, 47–57. [CrossRef]
22. Zhang, L.; Chen, Y.; Wan, Q.L.; Liu, T.; Zhu, J.F.; Tian, W. Electrochemical Corrosion Behaviors of Straight WC–Co Alloys: Exclusive Variation in Grain Sizes and Aggressive Media. *Int. J. Refract. Met. Hard Mater.* **2016**, *57*, 70–77. [CrossRef]
23. Ardila Téllez, L.C. Nuevos Recubrimientos Basados En Nitruros Con Adiciones de Silicio Para El Mecanizado de La Aleación Inconel 718 Con Herramientas de Metal Duro. Ph.D. Thesis, Universidad de Navarra, Pamplona, Spain, 2010.
24. Takadoum, J.; Houmid Bennani, H. Influence of Substrate Roughness and Coating Thickness on Adhesion, Friction and Wear of TiN Films. *Surf. Coat. Technol.* **1997**, *96*, 272–282. [CrossRef]
25. Croll, S.G. Surface Roughness Profile and Its Effect on Coating Adhesion and Corrosion Protection: A Review. *Prog. Org. Coat.* **2020**, *148*, 105847. [CrossRef]
26. Ghosh, G.; Sidpara, A.; Bandyopadhyay, P.P. Understanding the Role of Surface Roughness on the Tribological Performance and Corrosion Resistance of WC-Co Coating. *Surf. Coat. Technol.* **2019**, *378*, 125080. [CrossRef]
27. Leyland, A.; Matthews, A. On the Significance of the H/E Ratio in Wear Control: A Nanocomposite Coating Approach to Optimised Tribological Behaviour. *Wear* **2000**, *246*, 1–11. [CrossRef]
28. Charitidis, C.A. Nanomechanical and Nanotribological Properties of Carbon-Based Thin Films: A Review. *Int. J. Refract. Met. Hard Mater.* **2010**, *28*, 51–70. [CrossRef]
29. Charitidis, C.; Logothetidis, S.; Douka, P. Nanoindentation and Nanoscratching Studies of Amorphous Carbon Films. *Diam. Relat. Mater.* **1999**, *8*, 558–562. [CrossRef]
30. le Bourhis, E. Indentation Mechanics and Its Application to Thin Film Characterization. *Vacuum* **2008**, *82*, 1353–1359. [CrossRef]
31. Czyzniewski, A. Optimising Deposition Parameters of W-DLC Coatings for Tool Materials of High Speed Steel and Cemented Carbide. *Vacuum* **2012**, *86*, 2140–2147. [CrossRef]
32. Sun, W.; Li, M.; Wu, M.; Hu, J. Uniformity of Si-Containing Diamond-like Carbon Films Deposited at Different Positions by Mesh Hollow Cathode Discharge. *Results Phys.* **2019**, *14*, 102480. [CrossRef]
33. Wang, L.; Li, L.; Kuang, X. Effect of Substrate Bias on Microstructure and Mechanical Properties of WC-DLC Coatings Deposited by HiPIMS. *Surf. Coat. Technol.* **2018**, *352*, 33–41. [CrossRef]
34. Galvan, D.; Pei, Y.T.; de Hosson, J.T.M. Deformation and Failure Mechanism of Nano-Composite Coatings under Nano-Indentation. *Surf. Coat. Technol.* **2006**, *200*, 6718–6726. [CrossRef]
35. Hanner, L.A.; Pittari, J.J.; Swab, J.J. Dynamic Hardness of Cemented Tungsten Carbides. *Int. J. Refract. Met. Hard Mater.* **2018**, *75*, 294–298. [CrossRef]
36. Ciurans-Oset, M.; Mundó-Tijeras, I.; Mouzon, J.; Akhtar, F. Use of AFM Topography Images to Determine Microindentation Hardness of Cast Tungsten Carbide Powders. *Int. J. Refract. Met. Hard Mater.* **2022**, *107*, 105878. [CrossRef]
37. Srivatsan, T.S.; Woods, R.; Petraroli, M.; Sudarshan, T.S. An Investigation of the Influence of Powder Particle Size on Microstructure and Hardness of Bulk Samples of Tungsten Carbide. *Powder Technol.* **2002**, *122*, 54–60. [CrossRef]
38. Gao, Y.; Cai, F.; Lu, X.; Xu, W.; Zhang, C.; Zhang, J.; Qu, X. Design of Cycle Structure on Microstructure, Mechanical Properties and Tribology Behavior of AlCrN/AlCrSiN Coatings. *Ceram. Int.* **2022**, *48*, 12255–12270. [CrossRef]
39. Çam, A.S.; Ergüder, T.O.; Kaya, G.; Yıldız, F. Improvement of Structural/Tribological Properties and Milling Performances of Tungsten Carbide Cutting Tools by Bilayer TiAlN/TiSiN and Monolayer AlCrSiN Ceramic Films. *Ceram. Int.* **2022**, *48*, 26342–26350. [CrossRef]

40. Wu, Z.; Huan, J.; Geng, D.; Ye, R.; Wang, Q. Investigation on Plastic Deformation of Arc-Evaporated AlCrSiN and AlCrSiON Nanocomposite Films by Indentation. *Surf. Coat. Technol.* **2022**, *441*, 128570. [CrossRef]
41. Ziemath, E.C.; Herrmann, P.S.P. Densification and Residual Stresses Induced in Glass Surfaces by Vickers Indentations. *J. Non Cryst. Solids* **2000**, *273*, 19–24. [CrossRef]
42. Ashby, M.F.; Jones, D.R.H.; David, R.H. *Engineering Materials: An Introduction to Their Properties and Applications*; Pergamon Press: Oxford, NY, USA, 1980; p. 278.
43. Zhang, S.; Wang, L.; Wang, Q.; Li, M. A Superhard CrAlSiN Superlattice Coating Deposited by a Multi-Arc Ion Plating: II. Thermal Stability and Oxidation Resistance. *Surf. Coat. Technol.* **2013**, *214*, 153–159. [CrossRef]
44. Ćorić, D.; Šnajdar Musa, M.; Sakoman, M.; Alar, Ž. Analysis of Different Complex Multilayer PACVD Coatings on Nanostructured WC-Co Cemented Carbide. *Coatings* **2021**, *11*, 823. [CrossRef]
45. Claver, A.; Jiménez-Piqué, E.; Palacio, J.F.; Almandoz, E.; de Ara, J.F.; Fernández, I.; Santiago, J.A.; Barba, E.; García, J.A. Comparative Study of Tribomechanical Properties of HiPIMS with Positive Pulses DLC Coatings on Different Tools Steels. *Coatings* **2021**, *11*, 28. [CrossRef]
46. Su, Q.; Zhu, S.; Ding, H.; Bai, Y.; Di, P. Comparison of the Wear Behaviors of Advanced and Conventional Cemented Tungsten Carbides. *Int. J. Refract. Met. Hard Mater.* **2019**, *79*, 18–22. [CrossRef]
47. Doñu-Ruiz, M.A.; López-Perrusquia, N.; Renteria-Salcedo, A.; Flores-Martinez, M.; Rodriguez-De Anda, E.; Muhl, S.; Hernández-Navarro, C.; García, E. Tribocorrosion Behavior of Boride Coating on CoCrMo Alloy Produced by Thermochemical Process in 0.35% NaCl Solution. *Surf. Coat. Technol.* **2021**, *425*, 127698. [CrossRef]
48. Cao, S.; Mischler, S. A Lubricated Tribocorrosion Model Incorporating Surface Roughness. *Biotribology* **2021**, *26*, 100181. [CrossRef]
49. Hu, K.; Liu, X.; Zhang, S.; Xue, Z.; Yang, Y.; Yang, K. Tribocorrosion Behavior of HVOF Sprayed WC-Based Cermet Coatings in Sodium Chloride Solution Environment in Relation to Binder Phases. *Surf. Coat. Technol.* **2022**, *435*, 128248. [CrossRef]
50. Zhang, M.; Zhou, F.; Wang, Q.; Fu, Y.; Zhou, Z. Tribocorrosion Characteristics of CrMoSiCN/Ag Coatings on Ti6Al4V Alloys in Seawater. *Ceram. Int.* **2021**, *47*, 31780–31797. [CrossRef]
51. Boukantar, A.R.; Djerdjare, B.; Guiberteau, F.; Ortiz, A.L. A Critical Comparison of the Tribocorrosive Performance in Highly-Alkaline Wet Medium of Ultrafine-Grained WC Cemented Carbides with Co, Co+Ni, or Co+Ni+Cr Binders. *Int. J. Refract. Met. Hard Mater.* **2021**, *95*, 105452. [CrossRef]
52. Ouyang, Y.; Chen, Z.; Jiang, C.; Yang, W.; Chen, Y.; Yin, X.; Liu, Y. Design of the Double-Layer Biocompatible Coating on AZ31 Magnesium Alloy for Highly Effective Corrosion Resistance. *Surf. Coat. Technol.* **2021**, *428*, 127897. [CrossRef]
53. Sutthiruangwong, S.; Mori, G. Corrosion Properties of Co-Based Cemented Carbides in Acidic Solutions. *Int. J. Refract. Met. Hard Mater.* **2003**, *21*, 135–145. [CrossRef]